

SUNFLOWER

“Sustainable Novel Flexible Organic Watts Efficiently Reliable”

Grant agreement No.: 287594 (Integrated Project)

Deliverable D4.5:

Local correlation of ageing processes with morphological, compositional and functional changes

Due date of deliverable: 31 September 2014
Actual submission date: 14 October 2014

Start date of project: 1st October 2011

Duration: 48 months

Coordinator	CSEM
Deliverable Leading Partner	CNR
Contributing Partners	
Task	T 4.5
Revision	Belectric, LiU

Project co-funded by the European Commission under the Seventh Framework Programme (FP7)		
Dissemination Level		
PU	Public	PU
PP	Restricted to other programme participants (including the Commission Services)	
RE	Restricted to a group specified by the consortium (including the Commission Services)	
CO	Confidential, only for members of the consortium (including the Commission Services)	

Table of Contents

List of Figures and Tables.....	3
Abbreviations.....	4
1. Introduction.....	5
1.1 Purpose of this report.....	5
1.2 Description of the deliverable.....	5
2. Methodology.....	6
2.1 LSCM and basic concepts	6
3. Device fabrication and ageing process	9
3.1 Materials and device architectures.....	9
3.2 Polymer 1 (P1): Thermal degradation and correlation between OPV performance and morphological changes.....	10
3.2.1 Evolution of the photovoltaic parameters in standard and inverted structures of P1:PC₆₁BM based OPV.....	10
3.2.2 Morphological investigations by LSCM and AFM on P1:PC₆₁BM films.....	12
3.3 Polymer 2 (P2): Thermal degradation and correlation between OPV performance and morphological changes.....	17
3.3.1 Evolution of the photovoltaic parameters in inverted structures of P2:PC₆₁BM based OPV.....	18
3.3.2 Morphological investigations by LSCM and AFM on P2:PC₆₁BM film.....	19
4. Conclusions.....	21
5. References.....	22

List of figures and Tables

FIGURES

Figure 1: Schematic representation of a confocal fluorescence microscope.....	6
Figure 2: Collection of the signal (reflection mode) in a complete OPV device.....	7
Figure 3: Device structures: A) standard, B) inverted.....	10
Figure 4: OPV curves of “fresh” and thermally degraded standard P1:PC₆₁BM based cell.....	11
Figure 5: OPV curves of “fresh” and thermally degraded inverted P1:PC₆₁BM inverted based cell.....	12
Figure 6: Investigation by LSCM of different regions of a complete device (inverted architecture).....	13
Figure 7: A-F) AFM and; G-J) LSCM images, OUTSIDE THE ELECTRODE , of P1:PC₆₁BM based film during thermal degradation.....	14
Figure 8: LSCM images, UNDER THE ELECTRODE , of P1:PC₆₁BM based films during thermal degradation. Black arrows indicate enriched-PC ₆₁ BM domains; green arrow indicates enriched-polymer region.....	15
Figure 9: Localized emission spectra on P1:PC₆₁BM films during the degradation: A) “fresh” P1:PC₆₁BM film (under the electrode); B) P1:PC₆₁BM film after 150 h at 85°C (under the electrode); C) P1:PC₆₁BM film after 150 h at 85°C (outside the electrode).....	16
Figure 10: OPV curves of “fresh” and thermally degraded inverted P2:PC₆₁BM based cell.....	18
Figure 11: A-D) AFM images of P2:PC₆₁BM based devices before and after thermal degradation (240 h at 65°C); E-F) LSCM images, UNDER THE ELECTRODE , of P2:PC₆₁BM based films before and after thermal degradation (240 h at 65°C).....	20

TABLES

Table 1: OPV performance vs time of P1:PC₆₁BM based cells in standard configuration.....	10
Table 2: OPV performance vs time of P1:PC₆₁BM based cells in inverted configuration.....	11
Table 3: OPV performance vs time of P2:PC₆₁BM based cells in inverted configuration.....	18

Abbreviations

OPV	Organic Photovoltaic
BHJ	Bulk-heterojunction
PCE	Power Conversion Efficiency
PEDOT:PSS	(Poly(3,4-ethylenedioxythiophene) Polystyrene sulfonate
ITO	Indium Tin Oxide
AFM	Atomic Force Microscopy
LSCM	Laser Scanning Confocal Microscopy
HTL	Hole transporting layer
ETL	Electron transporting layer

1 Introduction

1.1 Purpose of this report

Competitive organic solar cells are not only required to be efficient, they also need to show decent lifetimes. In this contest, the aim of WP4 is to characterize the stability of organic solar cells, to identify and narrow down the source of failure in OPVs, and to develop methods for estimating their lifetime (e.g., see D4.2). Several advanced techniques have been employed to investigate and provide information on the sources of degradation of OPV cells. In addition, Fluxim in collaboration with Belectric and CSEM, respectively, have already used their all-in-one electrical characterization platform PAIOS and the simulation software SETFOS to determine degradation induced doping as well as stress-induced reduction of effective area of P3HT:PC₆₁BM based solar cells.

This report is mainly focused on the evaluation of the morphological changes of different polymer solar cells, after ageing process, by specific techniques: Laser Scanning Confocal Microscopy (LSCM) combined with Atomic Force Microscopy (AFM). Accelerated lifetime testing of OPV devices have been performed following different standard protocols. Firstly, the response of the resulting devices was characterized via current-voltage characteristics; secondly, the above mentioned advanced techniques have been used to demonstrate a correlation between degradation of device performance and physical changes in the device. In particular, we investigated the stability of the morphology, identifying specific properties/features in different regions of the active blend before and after degradation. In addition, this methodology has been applied on different devices based on different photoactive polymers in order to demonstrate the versatility and potential of the LSCM technique, independently from the materials and their degradation rate (related to the selected conditions).

1.2 Description of the deliverable

The failure mechanisms of artificially aged OPV devices are characterized (based on tests defined in D4.2). The key targets of the deliverable are:

- Effect of the ageing process on the morphology of the active layer and correlation with the corresponding OPV responses
- Role of the device architecture
- Identification of the main limiting factors for the device stability. Input given to WP2/WP1.
- To provide information/recommendations to reduce/control the failure locations

2 Methodology

2.1 LSCM and basic concepts

In organic BHJ solar cells, the correlation between the sub-micrometric morphology and device operation is of fundamental importance due to the intrinsic characteristics of a BHJ. Here, the optimal morphology should result in a fine intermix of the electron donor (D) and acceptor (A) domains, with sizes that meet the compromise between the D and A exciton diffusion lengths and a high D/A interfacial area, together with the need of bicontinuous percolation pathways for charges transport at the electrodes. The understanding of the correlation morphology/device operation could help to design the chemical structure of the active materials, or to modify the active layer processing (solvents, additives, temperature, deposition technique), in sight of obtaining the device optimal efficiency. Moreover, the evolution of the sub-micrometric morphology during the ageing of the cells could help to better understand the processes leading to the loss of the photovoltaic performances of the cells with degradation.

To date, spatially resolved photocurrent mapping¹, X-ray microscopy², conductive atomic force microscopy (cAFM)³, electrostatic force microscopy (EFM)⁴, combined photocurrent and fluorescence imaging⁵, and combined photocurrent and Raman spectroscopy⁶ have been employed to study the interplay between morphology and device operation in solar cells. Nevertheless, within all these techniques, confocal fluorescence microscopy⁷ presents several advantages: *i*) it allows to study the morphology of the active layer in the bulk (it is not a superficial technique such as AFM, TEM, SEM, etc..) in the real device, under operating conditions; *ii*) it allows a resolution down to hundreds of nanometers; *iii*) it is a non-invasive technique, therefore it can be performed on functioning devices without damage⁸; *iv*) it is a fast and relatively simple technique.

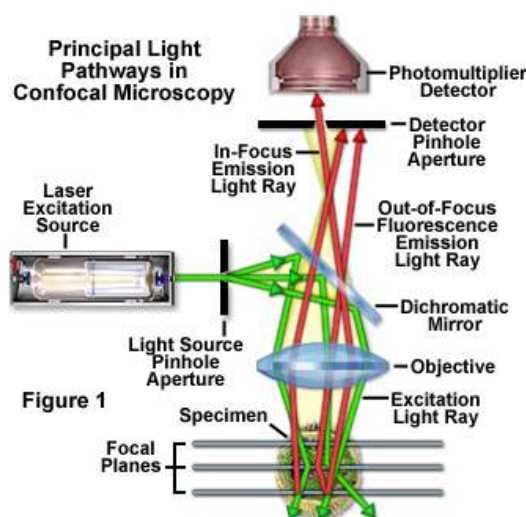


Figure 1. Schematic representation of a confocal fluorescence microscope.

In the confocal approach, comparing to conventional optical microscopy, spatial filtering is used to eliminate out-of-focus light or flare in specimens that are thicker than the plane of focus. A pinhole is placed in front of the excitation source as a point source of light. Light is reflected through a dichroic mirror towards an objective lens which focuses it onto the specimen. In confocal fluorescence microscopy (Figure 1), the signal detected is the emission of the excited specimen, acquired at the same focus as excitation (confocal). The

light emitted by the specimen (fluorescence) passes through the same objective lens, is transmitted by the dichroic mirror and passes through the second pinhole having the same focus as the first pinhole. Any light that passes the second pinhole is collected by a low-noise photomultiplier, which generates a signal related to the fluorescence intensity of the specimen. In laser scanning confocal fluorescence microscopy, a laser is used as excitation source. Moreover, to build a two-dimensional map of the photoluminescence of a specimen, the focused spot of light is moved in the x-y plane across the specimen (laser scanning). The final resolution achieved by the instrument is governed by the wavelength of light, the objective lenses, and the properties of the specimen itself.

The described laser scanning confocal fluorescence microscopy is used to study the thermal degradation in inert atmosphere of optimized solar cells. In particular, the scope is to correlate the morphological changes of the active layer with the change of the photovoltaic performances of the device occurring with thermal degradation. The devices are illuminated through the glass/ITO side under the metal electrode, and the photoluminescence signal is collected in reflection mode, as illustrated in Figure 2.

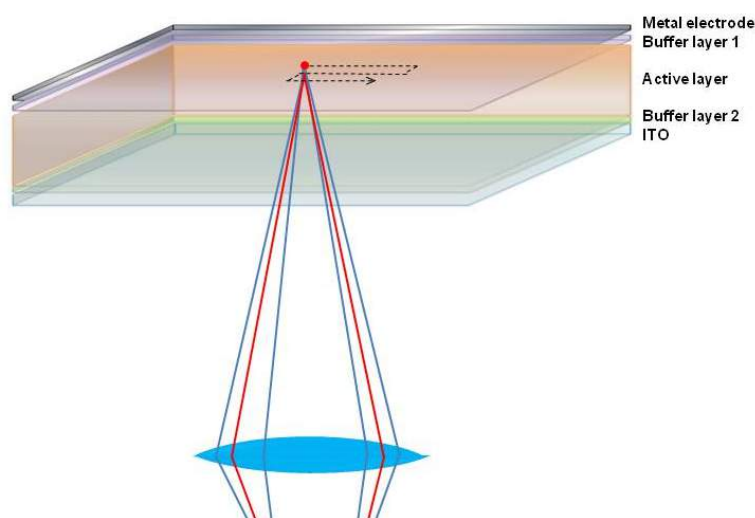


Figure 2. Collection of the signal (reflection mode) in a complete OPV device.

With the 405 or 488 nm laser excitation, light is absorbed by the donor polymer in the active layer. Even though most part of the polymer emission in the BHJ is quenched by the electron transfer process to the fullerene acceptor, it is still

possible to distinguish the morphological features of the active layer by collecting the residual photoluminescence from the polymer first excited singlet state (S_1). In some cases, it could be possible to detect, instead, the photoluminescence of the charge transfer state (CT), if this is an emissive state. The solar cells are studied at different degradation stages (at time 0, after 75, 150 or 240 h) and their fluorescence maps are compared and combined with AFM images.

For a more detailed analysis on the physical nature of the emissive species forming the photoluminescence map, the emission spectra at different points of the map can be registered (Figure 9). In this way it could be possible to distinguish, through their different spectral features, domains of pure polymer or pure fullerene formed by segregation from the blend during thermal degradation. In the same way, it could be possible to distinguish areas where the blend itself deteriorates. For the localized spectral analysis, the scanning head is fixed at a certain (x,y) position on the specimen (on the map) and the photoluminescence signal coming from the confocal microscope optics is transmitted, through an optical fiber and a couple of focusing achromatic lenses, to an optical multichannel analyzer (instead of the low-noise photomultiplier).

In addition, we recently tested the possibility to perform electroluminescence microscopy with the same apparatus as the confocal fluorescence microscope. The principle of electroluminescence imaging is based on inverting the operation mode of solar cells by injection of charge carriers under application of a forward bias using a current or voltage

source. Although being not optimized for light emission, part of the recombination of injected charge carriers will be radiative, resulting in the detection of photons emitted from the photoactive semiconductor. The same physical processes that influence the photovoltaic performance, such as recombination, resistive and optical losses, are also involved in the electroluminescence emission properties.

One advantage of combining the two luminescence imaging techniques is the discriminative characterization depending on the excitation mechanism. Fluorescence reflects the properties of the active blend alone. In contrast, electroluminescence, based on injection of charge carriers into the organic semiconductor from the two respective electrodes involved, gives information also on the conditions of the electrodes and on the electrode/organic layer interface.

Finally, we also tested the possibility to register the localized photocurrent of the solar cell by measuring it in short circuit during the illumination with the focalized laser from the microscope. The correlation of the photocurrent map with the confocal fluorescence images would constitute an additional technique useful to correlate the morphology/performance of complete devices before and after degradation.

The assembly of these two additional setups is in progress.

3 Device fabrication and ageing process

In this section we describe the part of the work concerning the device fabrication, in terms of specific active/functional materials and architectures, and the ageing process.

Degradation of “protected” (encapsulated or stored in inert atmosphere, glove-box) organic solar cells cannot be attributed to a single mechanism. The different processes leading to degradation in OPVs can be classified into three general categories. The first category is light-induced burn-in degradation. This degradation is characterized by an exponential drop of about 20% of the initial efficiency and most of it occurs in the first 200 hours. This is found to be caused by photo-induced traps and is independent of the electrodes and the amount of injected current. This can be mainly ascribed to: i) cross-linking and, ii) light-induced breaking of C–H bonds. The second category of degradation is long term degradation which is characterized by a slow, linear degradation, known as long-term degradation. A third category is thermal burn-in and is characterized by an exponential drop in efficiency that stabilizes over time. Thermal degradation appears to be related to the interfaces/interactions between different materials: organic/organic, organic/metal oxide, etc... In this work, following the procedures established in D4.2, we focus the attention on the thermal degradation and in particular on the control of the morphological evolution, by LSCM and AFM, of the BHJ blend during a continuous thermal annealing in inert atmosphere (inside the glove-box). The use of inert atmosphere allowed us to exclude the effect of environmental agents such as oxygen and water on the degradation mechanisms.

To this end, two different photoactive polymers have been used to fabricate BHJ solar cells and locally investigate the morphological changes before and after thermal degradation.

3.1 Materials and device architectures

As above mentioned, it is now recognized that OPV cell stability correlates with interface material issues, morphological stability of the OPV blend and the photodegradation of organic materials. These aspects require careful investigation in order to obtain stable organic solar cells. Here, the morphological stability/changes of the BHJ blend is the subject of study. In particular, BHJ solar cells that embed fullerene derivatives should be intrinsically unstable due to spontaneous phase segregation tendency of fullerene domains, resulting in PCE losses because of reduced charge separation and increased exciton recombination. In this contest, the optimization of the polymer structure and the tuning of the intermolecular interactions in the solid state (polymer-polymer, fullerene-fullerene and polymer-fullerene) play a crucial role for the stabilization of the BHJ morphology and thus the resulting lifetime of the corresponding devices.

To this aim, the effect of continuous thermal annealing on the BHJ morphology and power conversion efficiency of devices based on two different photoactive polymers has been studied. The polymers are coded as P1 and P2.

In addition, two different device architectures, STANDARD and INVERTED (Figure 3A and 3B, respectively), have been employed in order to evaluate how the electrodes nature and interfacial properties affect the thermal stability of the entire device.

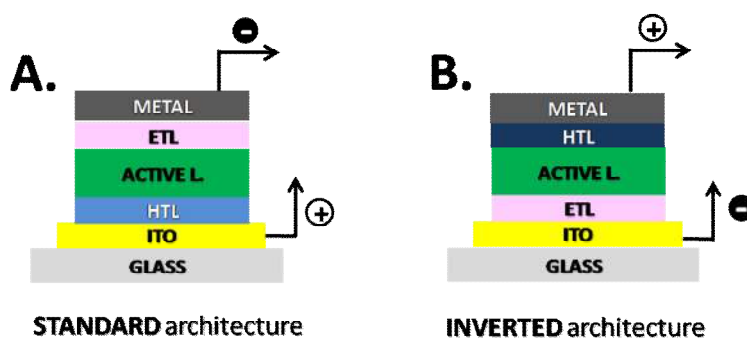


Figure 3. Device structures: A) standard, B) inverted

The cells contain the following layers from bottom to top:

- *STANDARD*: glass / ITO / PEDOT:PSS(AI4083) / active layer / ZnO(MG91) / Al
- *INVERTED*: glass / ITO / ZnO(MG91) / active layer / MoO₃ / Ag

3.2 Polymer 1 (P1): Thermal degradation and correlation between OPV performance and morphological changes

3.2.1 Evolution of the photovoltaic parameters in standard and inverted structures of P1:PC₆₁BM based OPV

In this section, the effect of continuous thermal annealing at 85 °C (on hot-plate in glove-box) on the photovoltaic responses of different OPV devices, based on P1 and using different architectures, is studied. Note that, this mild temperature (from 65°C to 85°C) has been defined as a reference temperature for OPV cell stability evaluation.⁹

Table 1 summarizes the photovoltaic responses of single layer BHJ cells based on P1:PC₆₁BM in standard configuration as a function of the degradation time (at 25°C and 85°C).

- *Thermal degradation of P1:PC₆₁BM using single layer cells in STANDARD configuration.* Glass / ITO / PEDOT:PSS(AI4083) / active layer / ZnO(MG91) / Al (Figure 4)

Table 1. OPV performance vs time of P1:PC₆₁BM based cells in standard configuration.

Cell	OPV data	T = 0 h	T = 70 h	T = 160 h	ΔPCE (%)
Reference: at 25°C in glove-box	J _{SC} (mA/cm ²)	11.0	10.8	10.9	
	V _{OC} (V)	0.79	0.78	0.78	
	FF (%)	64	66	65	
	PCE (%)	5.6	5.5	5.5	- 3%
Test: at 85°C in glove-box	J _{SC} (mA/cm ²)	10.4	5.8	6.3	
	V _{OC} (V)	0.78	0.77	0.75	
	FF (%)	65	55	54	
	PCE (%)	5.3	2.5	2.6	- 51%

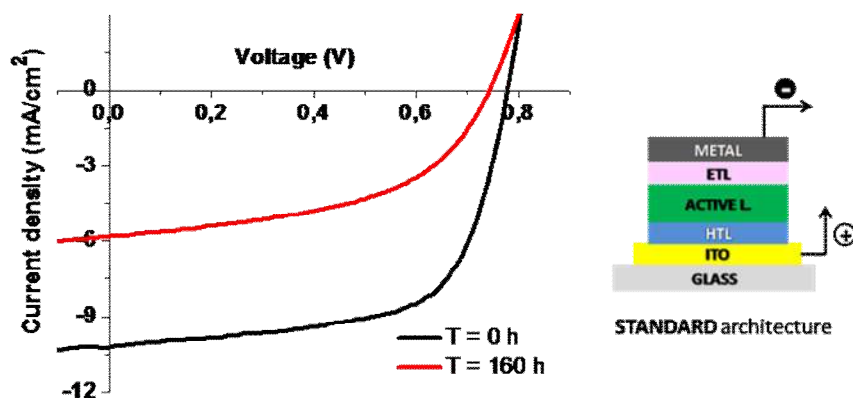


Figure 4. OPV curves of “fresh” and thermally degraded standard P1:PC₆₁BM based cell

Note that the performance of the reference system (stored at 25°C in glove-box) substantially does not change after 160 h (Δ PCE of ~ 3%), while the aged cell (heated at 85°C, always in glove-box) shows a drastic reduction of the PCE (Δ PCE of ~ 50%). In particular after 70 h we already observed a significant reduction of the PCE which could be related to a sub-optimal re-organization of the BHJ components, induced by the temperature, that limit the charge generation and transport in the active layer. Indeed, due to the almost amorphous nature of the active blend it is possible a demixing of the BHJ components resulting in a detrimental re-organization and/or phase segregation (in lateral and vertical device directions) that limit the electrical response of the blend, as confirmed by the simultaneous and drastic reduction of J_{SC} and FF (Table 2). Increasing the degradation time, from 70 h to 160 h, the situation does not change significantly indeed except a slight reduction in V_{OC} , J_{SC} , FF and PCE are almost maintained.

Nevertheless, the observed reduction of the OPV performance can be not only related to the active layer, indeed the presence of additional functional layers (e.g. PEDOT:PSS) and subsequent “critical” interfaces, ITO/PEDOT:PSS, could also play a key role during the thermal degradation. To this end, the inverted architecture, where different and more stable interlayers are used, has been studied to exclude this possible interference.

The corresponding OPV data, before and after thermal degradation, of analogous INVERTED BHJ solar cells are reported and discussed below.

- Thermal degradation of P1:PC₆₁BM using single layer cells in **INVERTED** configuration. Glass / ITO / ZnO(MG91) / active layer / MoO₃ / Ag (Figure 5)

Table 2. OPV performance vs time of P1:PC₆₁BM based cells in inverted configuration.

Cell	OPV data	T = 0 h	T = 50 h	T = 150 h	Δ PCE (%)
Reference: at 25°C in glove-box	J_{SC} (mA/cm ²)	10.8	10.3	10.3	
	V_{OC} (V)	0.77	0.77	0.77	
	FF (%)	68	68	68	
	PCE (%)	5.7	5.4	5.4	-5%
Test: at 85°C in glove-box	J_{SC} (mA/cm ²)	11.7	10.9	10.5	
	V_{OC} (V)	0.77	0.78	0.78	
	FF (%)	71	62	58	
	PCE (%)	6.4	5.3	4.8	-25%

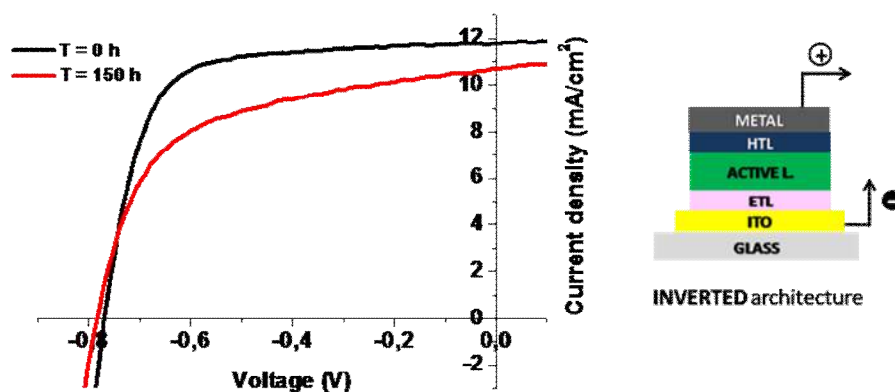


Figure 5. OPV curves of “fresh” and thermally degraded inverted P1:PC₆₁BM based cell

To evaluate the influence of the device architecture on the thermal stability, we fabricated inverted solar cells using the same active and functional layers (P1:PC₆₁BM and ZnO (MG91)) previously studied. The resulting OPV data are summarized in Table 2.

To note, for inverted devices the thermal stability is relatively improved. In fact, after 150 h at 85°C the PCE is reduced of ~ 25%, which is not enough to define stable the materials in accordance to D4.2 (the reduction has to be lower than 10%) but is still a significant improvement if compared to the analogous device with standard structure (see Table 1, Figure 4). This confirms a first key role in the ETL and HTL layers on the stability of the solar cell. The absence of PEDOT:PSS in particular could be responsible of the enhanced stability of the device, due to the suppression of the degradation processes known from literature.¹⁰

In addition, it is known¹¹ that the enhanced thermal stability of inverted cells, compared to standard devices, could be ascribed to a vertical phase segregation of the D:A blend¹² (also observed in D2.3) induced by the temperature, resulting in a larger amount of polymer close to the hole-collecting top electrode, favoring the hole extraction from the active layer.

After 150 h at 85°C, we mainly observe a slight reduction of the J_{SC} and FF, and a modest increase of the voltage. However, looking at the shape of the corresponding J-V curves (Figure 5) it is evident (after 150 h at 85°C, red curve) an increase in the slope of the curve near the y-intercept after degradation. This is a common indication of a shunt current loss. The reduction of the shunt resistance can be related to an increase of charge recombination processes in the active layer as a result of a demixing of the BHJ components (increased D:A phase segregation). This degradation process, already hypothesized also for the devices in standard architecture, is supported by morphological investigations reported below.

3.2.2 Morphological investigations by LSCM and AFM on P1:PC₆₁BM films

Here we present the results obtained by confocal fluorescence microscopy, combined with AFM imaging, to correlate the morphological, photophysical and photovoltaic properties of the active layer. In particular, complete **inverted OPV cells** (“fresh” and thermally degraded/aged) based on P1:PC₆₁BM, were investigated to correlate the functional response with sub-micrometer properties of the active blend. It should be stressed once again that we selected the most stable architecture (inverted) in order to minimize the ageing effects due to the electrodes and organic/electrode interfaces, and identify the additional effects, critical points or failure mechanism of the active layer that still impact on the lifetime of the resulting OPV device.

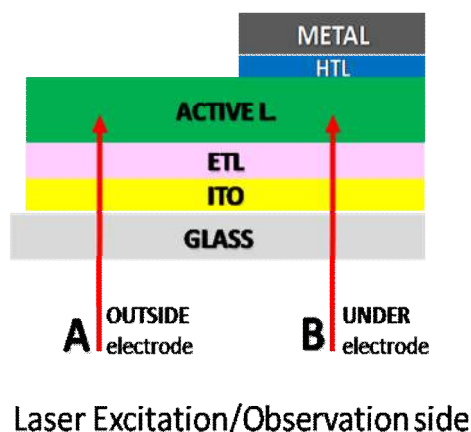


Figure 6. Investigation by LSCM of different regions of a complete device (inverted architecture)

Thank to the versatility of the LSCM technique, it is possible to investigate different regions of the devices, as depicted in Figure 6 (under and/or outside the top electrode, without damaging the device), in order to evaluate the effect of the interactions at the organic/electrode interface on the stabilization of the morphology and subsequently on the degradation processes involved, as discussed below. In fact the AFM technique, even though having a higher resolution if compared to LSCM, allows to study the surface features of the active layer surface only in the region outside the electrode.

The evolution of the active layer morphology outside the electrode during the thermal degradation tests is reported in Figure 7. Note that the morphological investigations have been carried out directly on the working device (test device) reported in Table 2.

Figures 7A-F show AFM images of **P1:PC₆₁BM** based cells, having different size (5 μm x 5 μm and 20 μm x 20 μm), while figures 7G-J exhibit LSCM images, based on two-dimensional (2D) map of the photoluminescence of the specimen (see section 2.1). The different features of the 2D maps acquired with LSCM are related to the physical nature of the emissive species (in the bulk) generating the photoluminescence map. For this reason it is possible to evaluate, within the instrumental resolution, the composition of the active blend at different stages of thermal ageing, by distinguishing different domains enriched of donor (D, polymer), acceptor (A, fullerene) and/or finely intermixed D:A phases.

The “fresh” sample ($T = 0$ h, left column Figure 7, Figure A, D, G) exhibits an almost featureless active layer, with a fine self-organization of the BHJ components. Indeed, the AFM images reveal (Figures 7A and 7D) the absence of aggregates (very low surface roughness) and finely structured domains, which suggest an optimal intermixing and nanoscale phase separation of the BHJ components, reflected in PCE greater than 6% (Table 2). This kind of morphology is also evidenced by LSCM, (Figure 7G) where the absence of contrast features in the image (in perfect agreement with the AFM images) confirms the fine intermixing of the BHJ components and the absence of evident polymer- or fullerene-enriched domains.

Diversely, after 50 h at 85°C (on hot-plate in glove-box) the AFM reveals the formation of some aggregates (Figure 7B and 7E). In agreement with the AFM images, the corresponding photoluminescence map (Figure 7H) shows similar features, with the formation of isolated aggregates with similar dimensions. In particular there can be distinguished highly emissive spots (polymer-rich domains, white dot) or poorly emissive spots (fullerene-rich domains, dark dot). This indicates that at this stage of thermal ageing the active blend starts to change with formation of demixing regions.

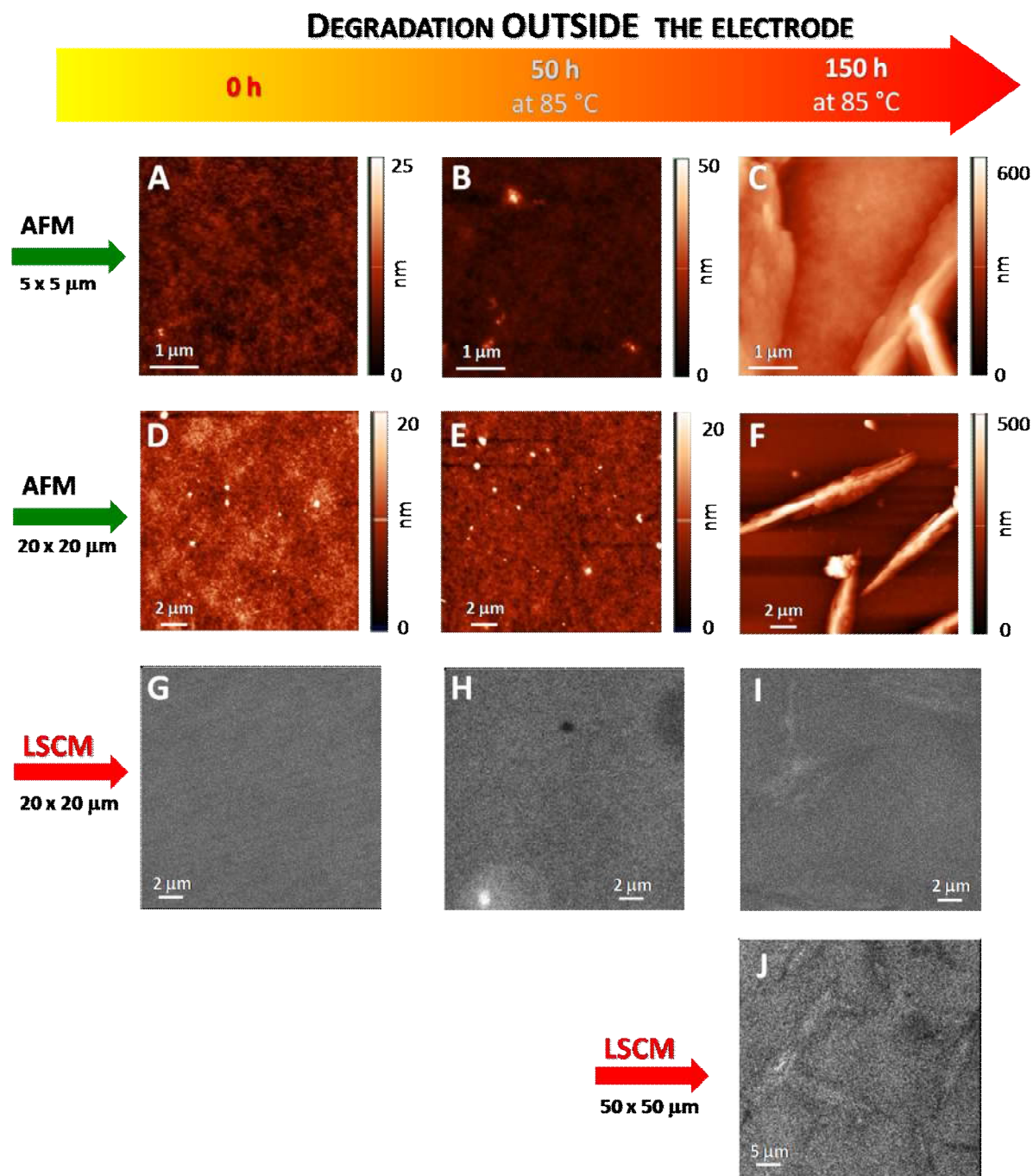


Figure 7. A-F) AFM and; G-J) LSCM images, **OUTSIDE THE ELECTRODE**, of P1:PC₆₁BM based film during thermal degradation.

After 150 h at 85°C the nanomorphology of P1:PC₆₁BM film drastically changes, with generation of large rod-like aggregates with dimensions of several micrometers as evidenced by AFM (Figures 7C and 7F). More precisely, it is evident in LSCM images (Figure 7I and 7J) the formation in the blend of domains with different composition: i) a homogeneous part of the blend reflects the initial situation with well intermixed BHJ components, and ii) rod-like regions, or crystals, enriched of aggregated polymeric chains.

After these findings and looking at the corresponding OPV results summarized in Table 2, it is “surprising” that, despite the observed drastic morphological changes occurring with

thermal ageing, the OPV performances of the cell are not so drastically reduced, as it could be expected. To this end, it is important to remind here that the morphological investigations reported in Figure 7 have been carried out in the region of the active layer outside the electrode (Figure 6). Even though we could suppose that the ageing processes of the active layer occurring outside the electrode area can be extended to the whole area, additional interactions can influence the morphological variations of the BHJ blend during ageing.

As previously mentioned, one of the advantages of LSCM technique is to allow the investigation of specific regions of the device not accessible with conventional techniques. Indeed, we completed the study on the morphology evolution during the thermal degradation (same devices: inverted P1:PC₆₁BM based BHJ cells) by investigating the region of the BHJ blend under the top electrode (without damaging the sample), which is directly the responsible of the photovoltaic process.

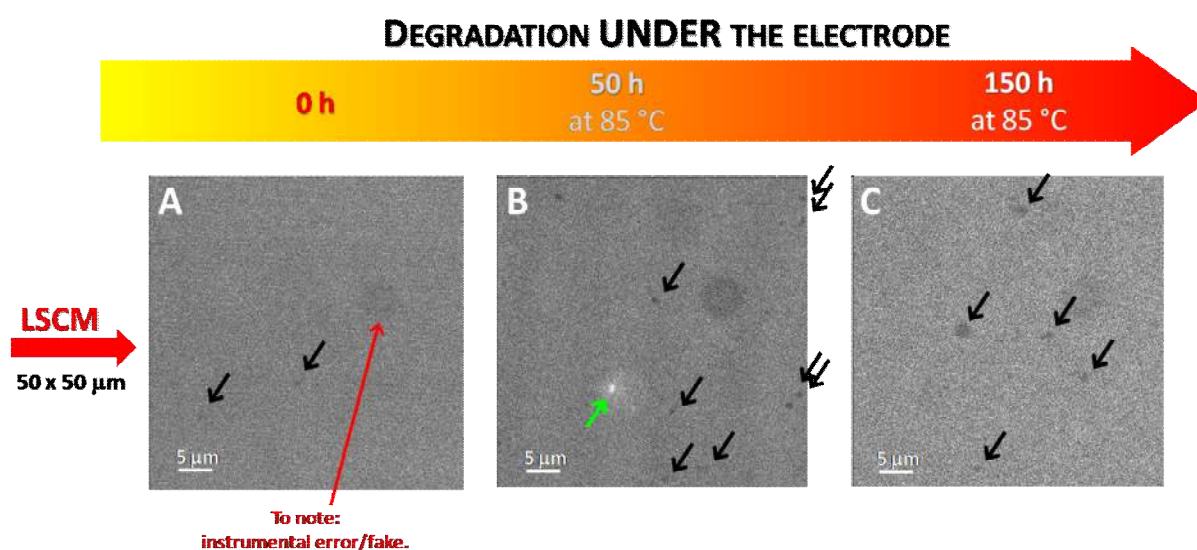


Figure 8. LSCM images, **UNDER THE ELECTRODE**, of P1:PC₆₁BM based films during thermal degradation. Black arrows indicate enriched-PC₆₁BM domains; green arrow indicates enriched-polymer region.

Figure 8 shows the evolution of the BHJ morphology, of P1:PC₆₁BM based cells, under the top metal electrode. It is evident the difference with the images collected outside the electrode (Figure 7G-J), in which we observed a predominant re-organization of the active blend with a strong D:A phase segregation occurring after 150 h (formation of rod-like aggregates). Diversely, under the electrode (Figures 8A-C) the kinetic of the polymer chains rearrangement seems to be strongly limited by the presence of the back electrode. In fact in the image of the aged cell, the formation of rod-like aggregates is not observed. This confinement/constriction effect given by the top electrode is most probably due to the interactions at the organic/metal oxide/metal interfaces, which result stronger than the polymer interchain ones acting as driving force for the formation of rod-like aggregates.

The dark spots observed in the LSCM images under the electrode (non-luminescent aggregates indicated by black arrows, Figure 8) can be ascribed to enriched-PC₆₁BM domains, which increase in number passing from the “fresh” to the 50 hours aged device, and increase in size but decrease in number with prolonged thermal degradation (150 h). This suggests a partial segregation of the fullerene molecules from the blend, in agreement with several reports.¹³

The limited effect of thermal degradation on the active layer morphology observed under the electrode in the inverted devices correlates well with the trend of the corresponding OPV performance. Indeed, this only partial degradation combined with a preferential vertical segregation of the polymer (the PCE of analogous devices with standard architecture decrease of 50%, Table 1), afford a final PCE of 5%, with a resulting Δ PCE of $\sim 25\%$ (Table 2).

For a deeper analysis on the partial demixing process (fullerene aggregation) occurring in the BHJ after thermal degradation, we report in Figure 9 the localized emission spectra performed on some representative luminescence 2D maps of P1:PC₆₁BM based devices. In particular, the spectra of the “fresh” and the thermally aged (150h) devices under the electrode, registered in localized areas (selection of specific points) of the 2D map, in the polymer/fullerene intermixed region, are reported. Since the emission quantum yield of fullerene derivatives is usually much lower ($<10^{-3}$) than the emission of highly conjugated polymers¹⁴, the PL spectra of the active layer has to be mainly ascribed to the polymer emission from its first excited singlet state (S₁).

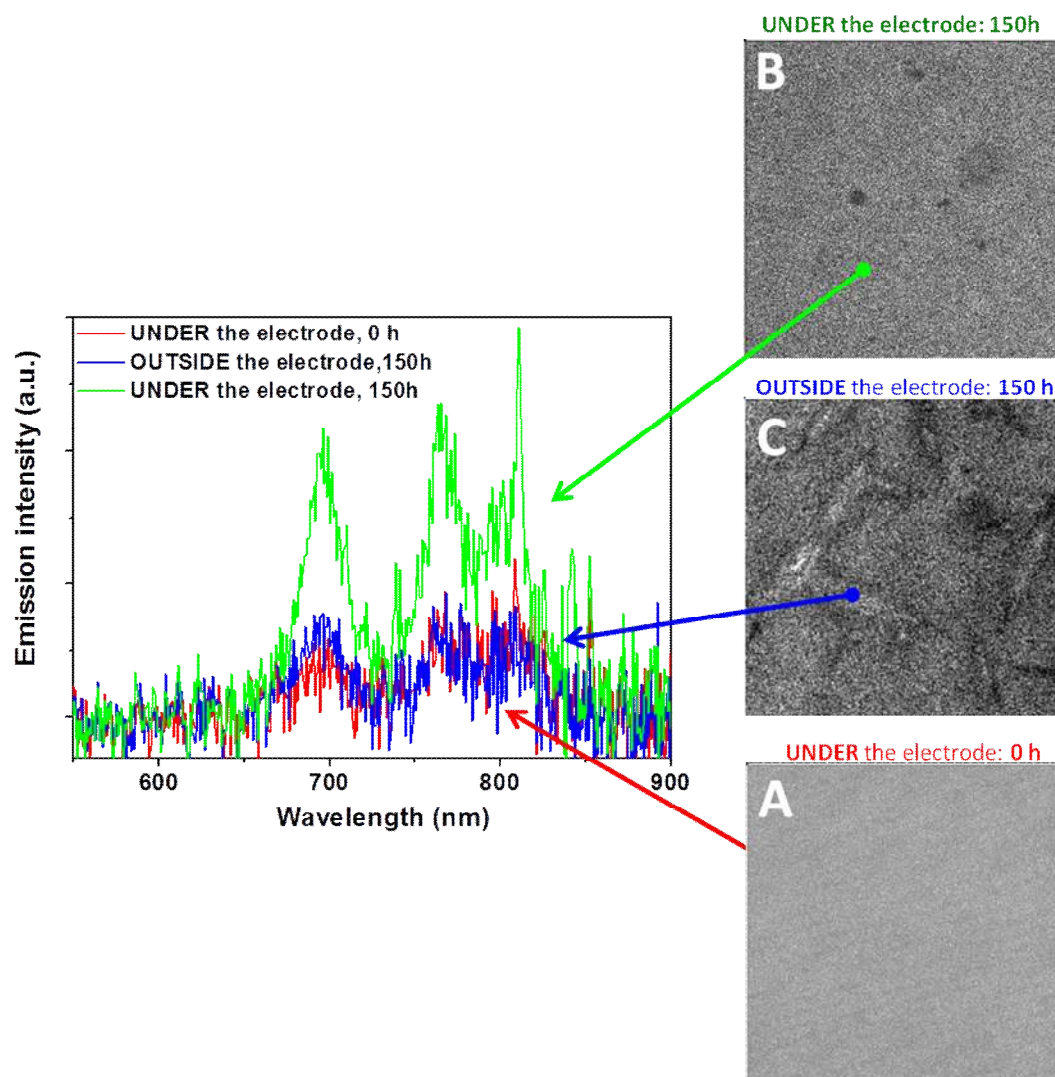


Figure 9. Localized emission spectra on P1:PC₆₁BM films during the degradation: **A**) “fresh” P1:PC₆₁BM film (under the electrode); **B**) P1:PC₆₁BM film after 150 h at 85°C (under the electrode); **C**) P1:PC₆₁BM film after 150 h at 85°C (outside the electrode)

In particular, the polymer photoluminescence is quenched in proportion to the electron transfer process to the fullerene acceptor: a higher emission relates to less efficient charge generation (lower quenching), while a lower emission is correlated to a more efficient charge generation (higher quenching). Indeed, the emission profile (barely detectable) in the intermixed area of the “fresh” device exhibits a lower intensity (Figure 9A and red spectrum) comparing to the emission in the intermixed area of the “aged” (150 h) device (Figure 9B and green spectrum). This confirms that the region of finely intermixed D:A domains in the aged device is poorer in PC₆₁BM and consequently the aggregates evidenced as black spots in the 2D map are PC₆₁BM aggregates, formed after the partial segregation of fullerene from the BHJ blend.

Note that the contrast (in Figure 9C) and the emission intensity (blue spectrum in Figure 9) of the polymer-enriched aggregates which form in the aged devices (150 h) outside the electrode is relatively low and comparable to the regions of the finely intermixed D:A domains. On the contrary, an enhancement of the intensity of the polymer emission should arise from the enhanced phase segregation and consequent decreased charge generation. Nevertheless, we should also take into account the self-quenching of the polymer photoluminescence occurring with the formation excimers in the ordered aggregates, which provide additional non-radiative decay pathways through the coupling of additional vibrational states.¹⁵ In this case, therefore, the two effects of decreased charge generation and increased self-quenching are balanced.

In conclusion, we demonstrated the morphological evolution, by LSCM, of P1:PC₆₁BM film during the thermal degradation (85°C for 150 h). We found a clear correlation between the morphological changes and the corresponding OPV response. Different regions of the film have been investigated and compared, highlighting the beneficial effect of the top electrode on the stabilization of the morphology.

To confirm the potential and the versatility of this methodology to monitor the morphological changes during ageing processes, we report in the next section an additional study applied to a relatively different context. Indeed, an inverted device based on a different photoactive polymer (P2) and thermally degraded using slightly different standard conditions⁹ (65°C for 240 h) has been investigated.

3.3 Polymer 2 (P2): Thermal degradation and correlation between OPV performance and morphological changes

In this section, we applied the same procedure/methodology to study a different photoactive polymer, coded as P2. As above mentioned, the goal is not to compare this material (P2) with the previous one (P1), but to apply this methodology to a different system in order to validate the versatility and potential of this technique.

To this end, inverted single layer solar cells based on P2:PC₆₁BM active blend have been prepared and their electrical and morphological properties have been monitored during the thermal degradation. Note that, we selected the inverted configuration due to the higher OPV performance, compared to analogous cells based on a standard architecture, which might highlight a preferential vertical phase segregation of the polymer which could be also beneficial during the thermal degradation¹¹ (see previous results and D2.3).

3.3.1 Evolution of the photovoltaic parameters in inverted structures of P2:PC₆₁BM based OPV

Table 3 summarizes the OPV performance of the P2:PC₆₁BM based cells. Note that, for this polymer we used slightly different conditions for the thermal degradation: a bit lower temperature for a longer time (65°C for 240 h (10 days)), which is still within the standard range established for testing thermal degradation⁹ (often used in literature¹¹). It should be stressed once again that we used a lower temperature (65°C) because it is a parallel and additional experiment, to monitor the morphological evolution of a different system, without aiming to compare the two photoactive polymers.

The OPV devices were kept on the hot-plate inside the glove-box.

- Thermal degradation of P2:PC₆₁BM using single layer cells in **INVERTED** configuration (Figures 10): glass / ITO / ZnO(MG91) / active layer / MoO₃ / Ag.

Table 3. OPV performance vs time of P2:PC₆₁BM based cells in inverted configuration.

Cell	OPV data	T = 0 h	T = 72 h	T = 165 h	T = 240 h	ΔPCE (%)
Reference: at 25°C in glove-box	J _{SC} (mA/cm ²)	9.7	9.5	9.5	9.4	
	V _{OC} (V)	0.85	0.84	0.84	0.84	
	FF (%)	53	53	52	52	
	PCE (%)	4.4	4.3	4.2	4.1	-6%
Test: at 65°C in glove-box	J _{SC} (mA/cm ²)	10.1	10.2	10.0	9.7	
	V _{OC} (V)	0.85	0.83	0.83	0.84	
	FF (%)	57	52	50	51	
	PCE (%)	4.9	4.3	4.2	4.2	- 14%

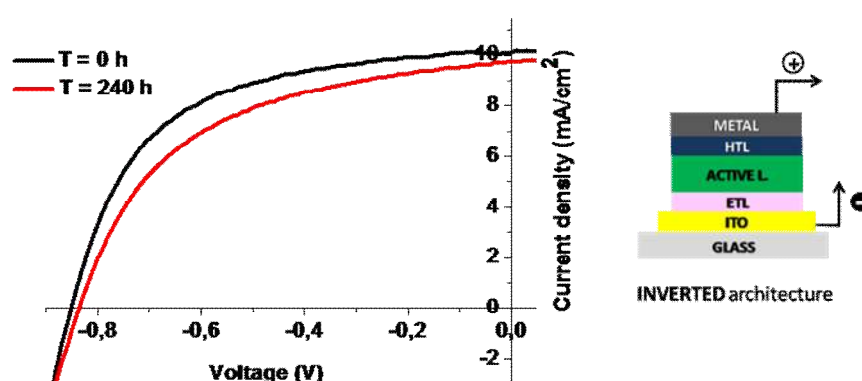


Figure 10. OPV curves of “fresh” and thermally degraded inverted P2:PC₆₁BM based cell

The trend of the OPV performance, summarized in Table 3, shows the relatively good thermal stability, at these conditions, of the polymer P2. Indeed, despite the decrease of 6% in PCE of the reference cell stored at RT in glove-box, the corresponding “aged” cell after 240 h at 65°C exhibits a reduction in PCE of only ~ 14% (from 4.9% to 4.2%). This variation is mainly ascribed to the decrease of the FF (from 57% to 51%), while the J_{SC} and V_{OC} values

are substantially maintained. Note that the most significant reduction of the OPV parameters mainly occur after the first 72 h, while remains nearly constant after that time. Observing the shape of the resulting J-V curves, before and after 240 h of thermal degradation (Figure 10), it is evident that the observed decrease in FF of the aged cell (red plot), is due to the reduced slope of the curve at the x-intercept, indicating an increase of the series resistance within the device (at higher voltages). The series resistance, R_S , represents the total resistance of the cell and it depends on several factors such as: i) the resistance at the donor/acceptor interface in the active layer (related to morphological changes); ii) the resistance at the active layer/ETL or active layer/HTL interfaces; iii) electrode resistances (degradation of the contacts/metals). The investigation of the morphological changes occurring in the active layer with thermal degradation, which are the main scope of this report, are discussed in the next section.

In conclusion, despite a Δ PCE of $\sim 14\%$ after 10 days at 65°C , the polymer P2 seems to be quite stable during thermal degradation at 65°C . In the next section we investigate the trend of the thin-film morphology (outside and under the electrode) that should reflect the OPV data.

3.3.2 Morphological investigations by LSCM and AFM on P2:PC₆₁BM films

Here we investigate, by LSCM combined with AFM, the morphological changes occurring with the thermal degradation processes in order to correlate this information with the OPV responses and eventually individuate failure locations induced by the thermal ageing.

In this case we investigated the nanomorphology of the active layer at $T = 0$ h and after 240 h at 65°C . Figure 11 shows the corresponding AFM and LSCM images.

The AFM images of the fresh P2:PC₆₁BM film (Figure 11A and 11C) reveal smooth and finely structured active blends with defined nanostructures, which suggest an optimal donor:acceptor intermixing. Similarly, after 240 h at 65°C , except for the formation of slightly more defined domains (Figure 11B and 11D), the surface morphology of the blend does not show significant changes, in agreement with the corresponding OPV performance.

The observed stability of P2:PC₆₁BM is also confirmed by LSCM images (Figure 11E and 11F) in which the absence of evident contrast features in both “fresh” and “aged” samples again reveals a high homogeneity in the composition of the active blend, as a result of finely intermixed BHJ components, without the formation of aggregates or segregated phases during the thermal degradation. Note that, the LSCM images have been taken in the region of the active layer under the electrode.

In conclusion the polymer P2 is relatively stable at 65°C after 240h and the slight variations at nanoscale level (not easily detectable) correlate well with the trend of the resulting OPV responses. Indeed, the modest reduction in FF can be ascribed to minimal adjustment or re-organization of the polymer/fullerene molecules which partially influence the charge transport, and thus the internal resistance, within the active layer.

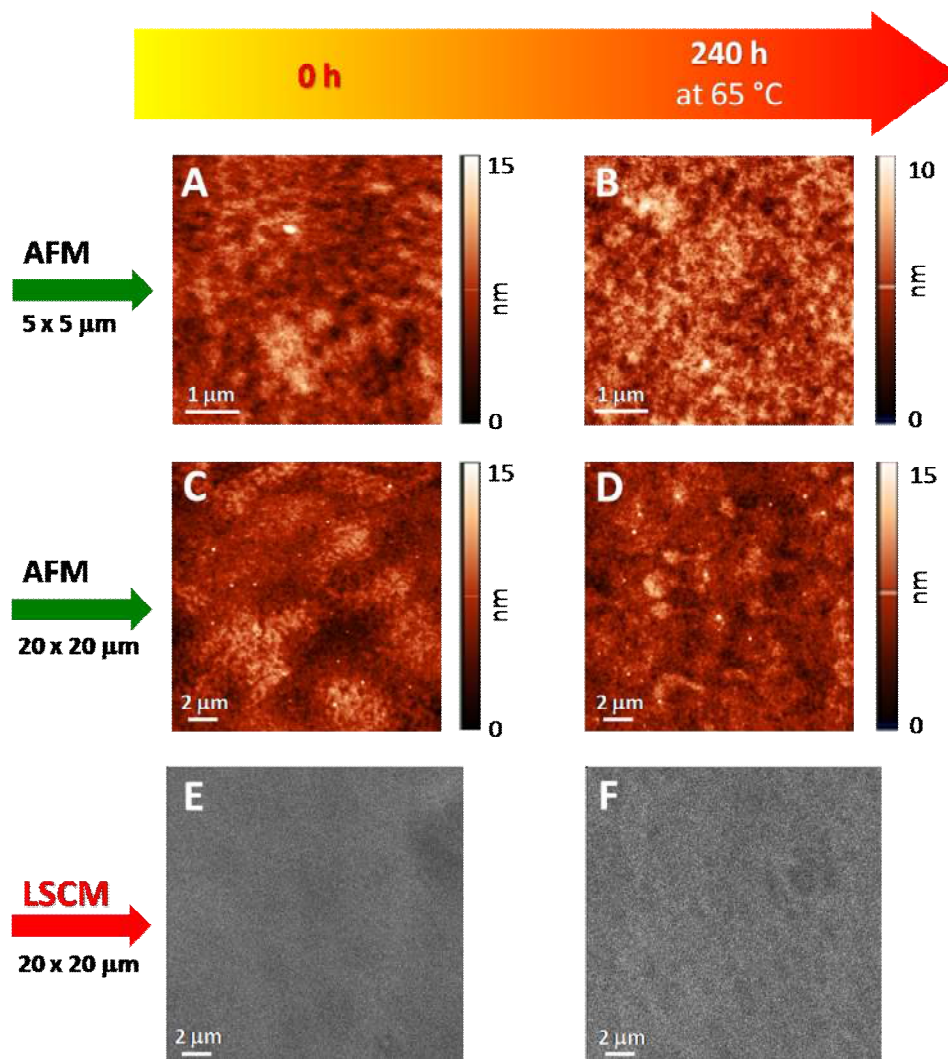


Figure 11. A-D) AFM images of P2:PC₆₁BM based devices before and after thermal degradation (240 h at 65°C); E-F) LSCM images, **UNDER THE ELECTRODE**, of P2:PC₆₁BM based films before and after thermal degradation (240 h at 65°C)

Once again, it is worth mentioning that the local morphological investigations such as AFM and LSCM correlate well with the observed electrical responses and help to identify/understand the failure mechanisms induced by the temperature. Of course, these data will be correlated and further implemented with complementary advanced techniques such as Impedance Spectroscopy (IS), Scanning Transmission Electron Microscopy (STEM), etc..., employed in WP4.

For the next future, we tested and validated the possibility to perform additional and complementary investigations using the same apparatus as the confocal fluorescence microscope: *i*) electroluminescence microscopy, and *ii*) localized photocurrent (or photocurrent map) on the solar cells.

4 Conclusions

The morphological stability, after thermal degradation (on the hot-plate in glove-box), of single junction BHJ solar cells based on different photoactive materials and thermal degradation processes was investigated. The corresponding OPV performances were monitored during the thermal treatment and the resulting data were correlated with the morphological changes in order to identify the critical aspects/processes that impact on the thermal stability. Moreover, for the polymer P1 two different device architectures, standard and inverted, were used and compared in terms of efficiency and stability. We found that the inverted devices show an enhanced stability. However, the active blend and in particular the donor polymer plays a crucial role on the stability of the corresponding device. In addition, we found that the interactions occurring at the organic/electrode interface (region under the top electrode) are determining for the stabilization of the morphology and subsequently for the degradation processes involved.

The morphological investigations on the above mentioned films were carried out by specific techniques: Laser Scanning Confocal Microscopy (LSCM) combined with Atomic Force Microscopy (AFM). In particular LSCM presents several advantages: *i*) it allows to study the morphology of the active layer in the bulk in the real device; *ii*) it allows a resolution down to hundreds of nanometers; *iii*) it is a non-invasive technique; *iv*) it is a fast and relatively simple technique; *v*) it allows to visualize the morphology under the electrode.

It is worth noting that the local morphological investigations such as AFM and LSCM correlate well with the observed electrical responses and help to identify/understand the failure mechanisms induced by the temperature, such as the demixing of the BHJ components and/or formation of aggregates/domains in different regions of the active blend. Of course, these data will be linked and further implemented with complementary advanced techniques such as Impedance Spectroscopy (IS), Scanning Transmission Electron Microscopy (STEM), etc..., employed in WP4.

For the next future, we tested and validated the possibility to perform additional advanced investigations (using the same apparatus as the confocal fluorescence microscope) such as electroluminescence microscopy and localized photocurrent (or a photocurrent map) of the solar cell to study additional processes linked to the charge generation/recombination.

5 References

1. C. R. McNeill, H. Frohne, J. L. Holdsworth, P. C. Dastoor, *Nano Lett.* **2004**, 4, 2503.
2. C. R. McNeill, B. Watts, L. Thomsen, H. Ade, N. C. Greenham, P. C. Dastoor, *Macromolecules*, **2007**, 40, 3263.
3. O. Douhéret, L. Lutsen, A. Swinnen, M. Bresselge, K. Vandewal, L. Goris, L. Manca, *Appl. Phys. Lett.* **2006**, 89, 032107.
4. D. C. Coffey, D. S. Ginger, *Nat. Mater.*, **2006**, 5, 735.
5. D. P. Ostrowski, M. S. Glatz, B. W. Goodfellow, V. A. Akhavan, M. G. Panthani, B. A. Korgel, D. A. Vanden Bout, *Small*, **2010**, 6, 2832.
6. Y. Gao, T. P. Martin, A. K. Thomas, J. K. Grey, *J. Phys. Chem. Lett.* **2010**, 1, 178.
7. T. J. K. Brenner and C. R. McNeill, *J. Phys. Chem. C*, **2011**, 115, 19364.
8. a) “*Stability and Degradation of Organic and Polymer Solar Cells*”, First Edition, Ed. Frederik C. Krebs., **2012** John Wiley & Sons, Ltd.; b) D. P. Ostrowski and D. A. Vanden Bout, *Small*, **2014**, 10, 1821.
9. M. O. Reese, S. A. Gevorgyan, M. Jørgensen, E. Bundgaard, S. R. Kurtz, D. S. Ginley, D. C. Olson, M. T. Lloyd, P. Morvillo, E. A. Katz, A. Elschner, O. Haillant, T. R. Currier, V. Shrotriya, M. Hermenau, M. Riede, K. R. Kirov, G. Trimmel, T. Rath, O. Inganäs, F. Zhang, M. Andersson, K. Tvingstedt, M. Lira-Cantu, D. Laird, Christine McGuinness, S. Gowrisanker, M. Pannone, M. Xiao, J. Hauch, Roland Steim, D. M. De Longchamp, R. Rosch, H. Hoppe, N. Espinosa, A. Urbina, G. Yaman-Uzunoglu, J.-B. Bonekamp, A. J.J.M.vanBreemen, C. Girotto, E. Voroshazi, F. C. Krebs; *Solar Energy Materials & Solar Cells*, **2011**, 95, 1253.
10. a) M., Manceau, A., Rivaton, J.-L., Gardette, J.-L., Guillerez, N., Lemaître, *Sol. Energy Mater. Sol. Cells.*, **2011**, 95, 1315; b) K., Kawano, R., Pacios, D., Poplavskyy, J., Nelson, D.D.C., Bradley, J.R., Durrant, *Sol. Energy Mater. Sol. Cells*, **2006**, 90, 3520; c) F. C., Krebs, J. E., Carle, N., Cruys-Bagger, M., Andersen, M. R., Lilliedal, M. A., Hammond, S., Hvidt, *Sol. Energy Mater. Sol. Cells*, **2005**, 86, 499.; d) M. Girtan, M. Rusu, *Sol. Energ. Mat. Sol. Cells*, **2010**, 94, 446.
11. I.T., Sachs-Quintana, T., Heumüller, W. R., Mateker, D. E., Orozco, R., Cheacharoen, S., Sweetnam, C. J., Brabec, M. D. McGehee, *Adv. Funct. Mater.*, **2014**, 24, 3978.
12. S. S. van Bavel, M. Bärenklau, G. de With, H. Hoppe, J. Loos, *Adv. Funct. Mater.*, **2010**, 20, 1458.
13. S. Bertho, G. Janssen, T.J. Cleij, B. Conings, W. Moons, A. Gadisa, J. D’Haen, E. Goovaerts, L. Lutsen, J. Manca, D. Vanderzande, *Sol. Energy Mater. Sol. Cells*, **2008**, 92, 753.
14. D. M., Guldi, M. Prato, *Acc. Chem. Res.* **2000**, 33, 695.
15. V. N. Bliznyuk and S. A. Carter, *Macromolecules*, **1999**, 32, 361.